JOURNAL OF Applied Polymer SCIENCE

Hydrothermal Aging Mechanisms of Aramid Fibers via Synchrotron Small-Angle X-ray Scattering and Dynamic Thermal Mechanical Analysis

Chang-Sheng Li,[1] Mao-Sheng Zhan,[1] Xian-Cong Huang,[2] Hong Zhou,[2] Yan Li[2]

[1]Key Laboratory of Aerospace Materials and Performance (Ministry of Education), School of Materials Science and Engineering, Beihang University, Beijing, China

[2]The Quartermaster Research Institute of the General Logistics Department of People's Liberation Army, Beijing, China

Correspondence to: M.-S. Zhan (E-mail: zhanms@buaa.edu.cn)

ABSTRACT: In this study, synchrotron small-angle X-ray scattering (SAXS) and dynamic mechanical thermal analysis (DMTA) were used to evaluate the aging behavior of microfibrils and nanovoids. The effects of such structures on the tensile strength were also investigated. We investigated the correlation length of the fibril interface by fitting the SAXS intensity using the Debye–Bueche method. The orientation and size of the voids were determined with Ruland's streak method. The results show that the correlation length decreased with aging time at 90°C. Voids formed after aging at high temperatures for prolonged periods. In addition, the orientation of the 10 Å voids changed with the degree of degradation. DMTA results revealed a new transition temperature for the aged fibers. A model based on the SAXS and DMTA results is proposed to illustrate the hydrothermal aging mechanism. © 2012 Wiley Periodicals, Inc. J. Appl. Polym. Sci. 128: 1291–1296, 2013

KEYWORDS: ageing; polyamides; properties and characterization; X-ray

Received 25 April 2012; accepted 30 July 2012; published online 8 October 2012
DOI: 10.1002/app.38419

INTRODUCTION

Kevlar 129 is a kind of aramid fiber that is widely used in body armors, ropes, and composites because of its high tensile modulus, high tensile strength, and low density. The crystalline structure,[1–3] skin–core morphology,[4–6] and defect layer of aramid fibers[4] have been studied extensively. Skin–core, fibrillar, and crystalline structure models have also been proposed. Aramid fibers can easily be hydrolyzed at high temperatures and humidities.[7–14] The core structure of the fiber consists of fibrils, bonding ties, defect zones, and interfaces between the crystals. The different structures may have different aging mechanisms in a hydrothermal environment.

The evolution of the structure and morphology during aging has been investigated through several methods, including X-ray diffraction,[1–3,15] dynamic mechanical thermal analysis (DMTA),[1,16] Fourier transform infrared spectroscopy,[7–14,17] viscosity measurements,[7–9] and scanning electron microscopy.[7,13] The results of these studies have indicated that the crystalline structure is not affected by aging; hydrolysis tends to occur in the bonding ties of the fibrils, and the tensile strength has a linear relationship with the viscosity. The fiber tends to break at defects with congregate chain ends. Synchrotron small-angle X-ray scattering (SAXS) has been widely used to study structures containing defects, such as long periods,[18–20] voids,[5,21–23] and fibrils.[19,24–27] However, few studies analyzing the hydrothermal aging behavior via SAXS have been reported. In this study, we used SAXS and DMTA to study the mechanisms of hydrothermal aging. The Debye–Bueche method and Ruland's streak method were applied to study the size of the fibrillar structures and voids. The effects of the temperature and time on such structures were also investigated. A potential model is proposed to illustrate the mechanisms at the different stages of aging.

EXPERIMENTAL

Materials and Aging Procedure

Kevlar 129 was used as a representative aramid fiber and was supplied by DuPont, Beijing, China. The average diameter of a single fiber is 12.26 μm. Hydrothermal aging was performed by the immersion of the fibers in deionized water at four temperatures: 60, 70, 80, and 90°C.

Measurements

Surface morphology was characterized via atomic force microscopy (AFM) with a Nanoscope (R) IV Digital Instruments from Veeco USA. Single fibers were fixed onto metallic discs

Applied Polymer SCIENCE

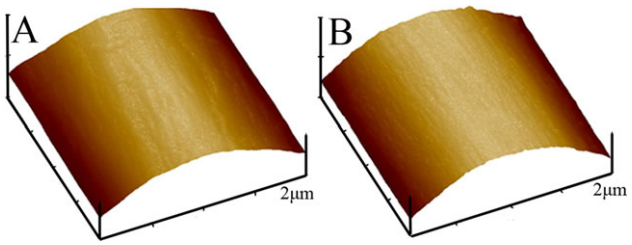

Figure 1. AFM images of the surface morphology of the aramid fibers: (A) as-received, and (B) 90°C/12 week. [Color figure can be viewed in the online issue, which is available at wileyonlinelibrary.com.]

12 mm in diameter with double-sided carbon adhesive tape and then mounted onto a microscopic stage. The tapping mode of operation was done via contact mode. Every sample was imaged on three different fibers and different areas to determine the reproducibility of the results.

DMTA of the single fibers was performed with a TA Q800 instrument from USA in the film tension mode at a frequency of 1.0 Hz and an amplitude of 40 μm. The temperature was programmed to increase from −80 to 120°C at a rate of 5°C/min.

SAXS measurements were performed at the beam line 1W2A at the Beijing Synchrotron Radiation Facility. The X-ray wavelength used was 0.154 nm. The sample was horizontally mounted in a sample holder at a sample-to-detector distance of 1.788 m. The Debye–Bueche method[22,28] was used to analyze the correlation length (L_c) with eq. (1). The scattered intensity from electron-density fluctuations in the phases was omitted in this study. L_c was determined from the slope and intercept of the plot of $[I(\mathbf{q})]^{-0.5}$ versus $\mathbf{q}^2$, where $\mathbf{q}$ is the scattering vector I is the intensity. The length of the microvoids was calculated with Ruland's streak method[21,22] [eq. (2)] with a Gaussian distribution function. B_ψ was used to estimate the orientation of the microvoids:

$$I(q) = \frac{I_0}{\left(1 + q^2 L_c^2\right)^2} \tag{1}$$

where I_0 is the intensity scaling factor.

$$B_{obs}^2 q^2 = B_\psi^2 q^2 + \frac{4\pi^2}{L^2} \tag{2}$$

where $\mathbf{q}$ is determined from the following relationship: $\mathbf{q} = 4\pi\sin\theta/\lambda$, where 2θ is the scattering angle; L is the scatter length; B_{obs} is the observed integral breadth of the azimuthal profile (along the fiber direction); and B_ψ is the integral breadth of the normals of the scatters.

RESULTS AND DISCUSSION

AFM Results

The fiber surface morphology before and after aging was characterized via AFM; the results are shown in Figure 1. The untreated fiber was slightly rougher than the aged fiber (90°C/12 weeks) because of the removal of the surface finish by water. The surface presented a morphological feature consisting of fibrils that were arranged parallel to the fiber direction. The fibril size was in the tens of nanometers. The size of the aged fiber fibrils seemed smaller than that of the untreated fibers. Both fiber surfaces showed no obvious defects. The difference in the surface morphologies of the untreated and aged fibers was small compared with the difference in their reduced viscosities (Table I). Thus, the surface morphology was not affected by hydrothermal aging; this was consistent with our previous scanning electron microscopy results.[29] The skin–core structure is one of the unique structures in aramid fibers. It was also proven that the skin and core have different evolutions of structure under hydrothermal environments. The deterioration of the tensile strength may have resulted from an inner defect, such as inner voids. This is illustrated by the SAXS results in the following text.

SAXS Results

The evolution of the fibril structure and that of voids during hydrothermal aging was evaluated via SAXS. As mentioned previously, the surface properties were not affected by aging; thus, the effect of the surface properties on the intensity of the SAXS results was negligible. The typical two-dimensional (2D) images of the untreated and aged fibers are shown in Figure 2. The fiber direction is parallel to the horizontal line. The vertical

Table I. Sample Tensile Strength, Nanostructure, and Microvoid Length

Sample name	Tensile strength (GPa)	Reduced viscosity (L/mg)	L_c (Å) Equatorial **q** 0.1–0.2	L_c (Å) Meridional **q** 0.1–0.2	Ruland steak method L (Å)	Ruland steak method B^ψ
As received	3.6	715	162.5	90.2	—	—
90°C/2 weeks	2.9	498	145.6	90.8	—	—
90°C/4 weeks	1.9	368	141.0	103.8	8.41	17.64
90°C/8 weeks	1.6	357	127.4	101.4	9.64	13.70
90°C/12 weeks	1.2	292	113.3	102.7	10.82	14.31
60°C/12 weeks	2.2	457	125.3	96.7	—	—
70°C/12 weeks	2.1	431	128.6	101.0	8.66	18.63
80°C/12 weeks	1.5	326	132.8	98.2	10.46	15.14

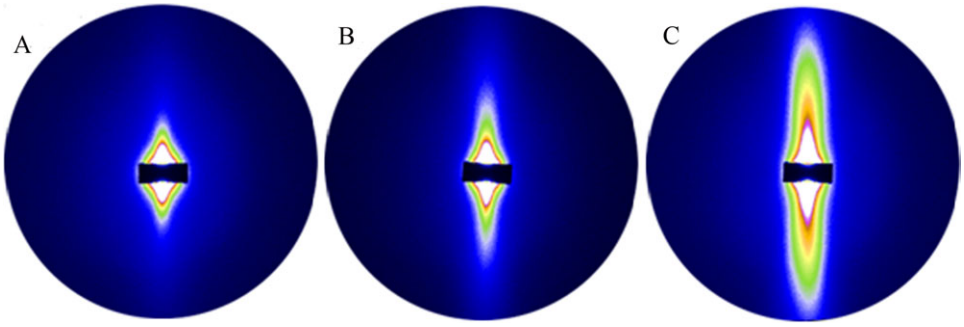

Figure 2. The typical 2D SAXS of the fiber before and after hydrothermal aging (A: As-received, B 90°C/4week, B 90°C/12week). [Color figure can be viewed in the online issue, which is available at wileyonlinelibrary.com.]

scattering intensity of the 2D patterns corresponds to the equatorial directional scatter of the fiber; thus, the horizontal intensity corresponds to the fiber direction (meridian direction). A remarkable difference between the untreated fibers and the aged fiber in the equatorial direction was observed. The evolution of such structures under different temperatures and time periods is discussed in the subsequent sections.

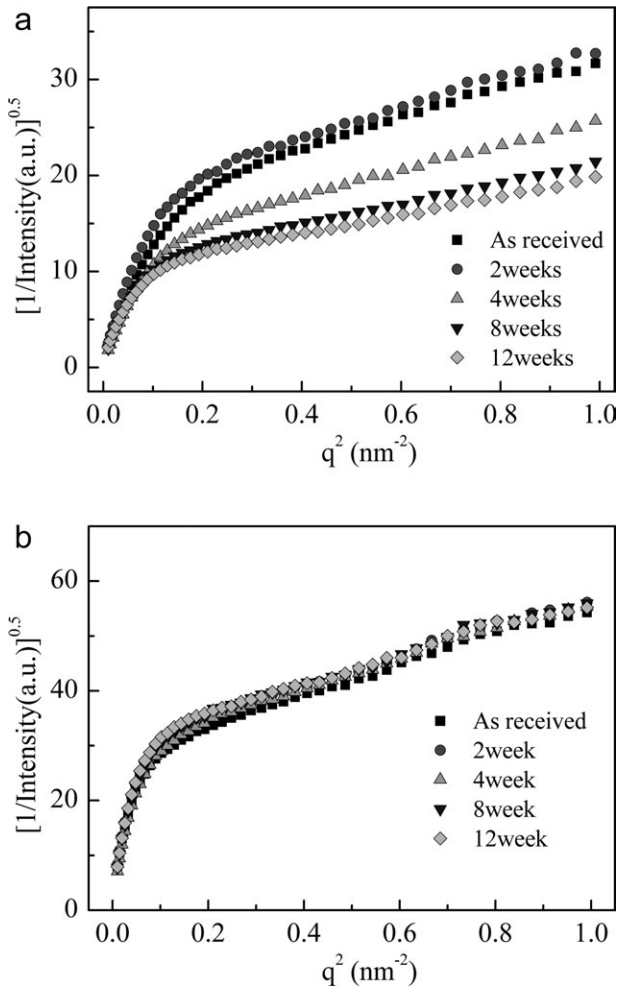

Figure 3. (A) Equatorial and (B) Meridian intensities as determined via Debye-Bueche analysis (90°C).

Figure 3 shows that the Debye–Bueche intensity plot for the equatorial direction was notably different from that for the meridian direction. The meridian intensity was completely independent of the aging time. No scatters formed in the fiber direction during aging. The equatorial intensity ($\mathbf{q}^2 > 0.2$) was stable during the first 2 weeks and subsequently increased with the aging time. L_c of the scatters is summarized in Table I. No correlation was found between L_c and the aging time, except for L_c ($\mathbf{q} = 0.1$–0.2); this decreased with the aging time. This length possibly corresponded to the size of the interface between the fibrils. In other words, it was attributed to the bonding ties between the fibrils. In a previous study,[30] the hydrolysis of the chain was believed to have originated from the bonding ties. Derombise et al.[11] also discovered the linear relationship between the tensile strength and reduced viscosity. It was believed that the hydrolysis started from the bonding ties.

The relationship between the intensity and the aging temperature (12 weeks) is illustrated in Figure 4. The meridian intensity was constant, whereas the equatorial intensity ($\mathbf{q}^2 > 0.2$) increased with the aging temperature. L_c ($\mathbf{q} = 0.1$–0.2) had no relationship with the aging temperature. These results suggest that a degradation mechanism other than hydrolysis of the bonding ties may have been involved in long-term aging.

Interestingly, the intensity was related to the aging time and the temperature at higher **q** values. The intensity at higher **q** values was associated with the smaller sized scatters. Grubb et al.[31] and Rana et al.[32] believed that the scatters in Kevlar 49 were associated with the microfibrillar structure rather than with the voids. This finding was consistent with the results obtained for the as-received fiber. In our previous work,[29] no void was observed with field emission scanning electron microscopy. However, the aged fibers in this study exhibited 2D patterns that were different from those of the as-received fibers. The pattern of the aged fibers was similar to that of carbon fibers and was an indicator of the formation of voids after aging.

The average length and orientation of the voids were calculated with Ruland's streak method; the results are presented in Figure 5 and Table I. The range applied in this method was from 0.4 to 1.0. The signal-to-noise ratio was low at higher **q** values, whereas the intensity was associated with the scatters at lower **q**. The as-received and 90°C/2 week fibers could not be fitted with Ruland's method; this indicated that only a small amount

Applied Polymer SCIENCE

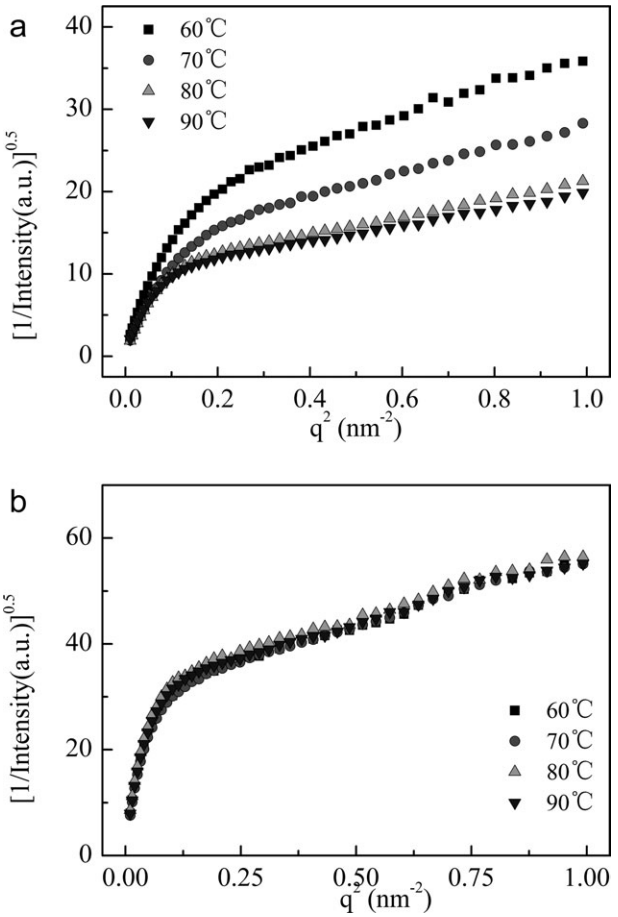

Figure 4. (A) Equatorial and (B) Meridian intensities as determined via Debye-Bueche analysis (12 weeks).

of voids were present in these fibers. The orientation of the voids changed with the degree of degradation. This behavior implied that the voids were derived from the interfaces of the amorphous region between the crystals and not from the bonding ties. It was proven by our WAXD results.[29] The crystallinity was not affect by hydrothermal aging.

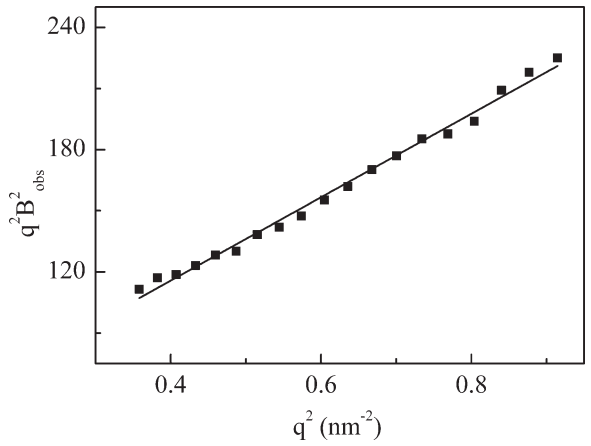

Figure 5. Length and orientation of the voids as calculated via Ruland's method.

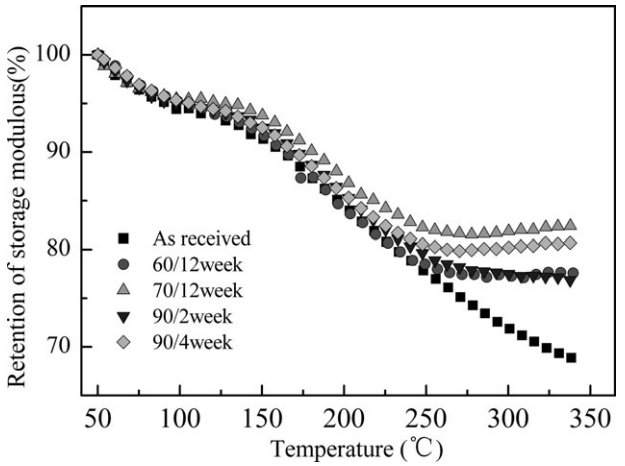

Figure 6. Storage modulus of the aramid fibers before and after aging.

DMTA Results

DMTA of the single fibers was conducted to study the relationship between the fiber structure and properties. The changes in the storage modulus and loss factor as functions of temperature are shown in Figures 6 and 7. The storage modulus was normalized by the modulus at 50°C to minimize the difference in the fiber diameters. Some aged samples were too weak to test; thus, only the high-strength retention fibers were analyzed. Interestingly, the storage modulus of the aged fibers leveled off around 250°C. This phenomenon was not observed in the untreated fibers and may have been a result of crosslinking in the chain. More chain ends were observed after degradation, and the bonding ties between the fibrils reformed when the temperature increased to 250°C. The transition temperature of the aged fiber was around 220°C. Rao et al.[1] assumed that the transition temperature was due to β relaxation in the crystalline region. They supposed that the mobility of the amorphous phase was enhanced by relaxation. Our results were consistent with such a hypothesis. The crystallinity degree did not change after aging.[29] The voids formed only in the amorphous phase. This suggested that the hydrolysis happened in the amorphous region.

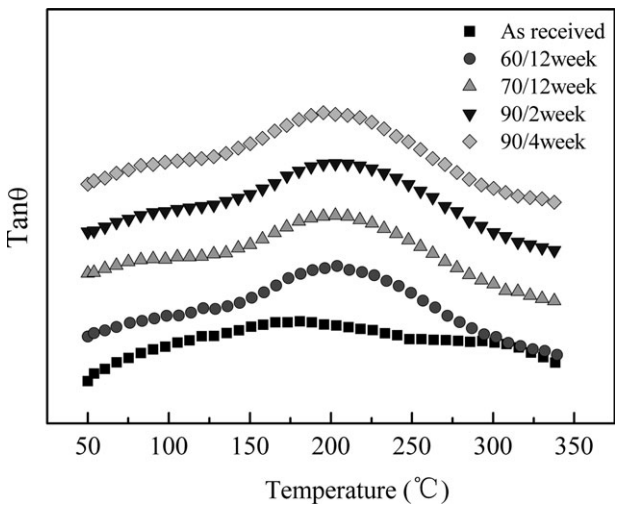

Figure 7. The loss factor of aramid fibers before and after aging.

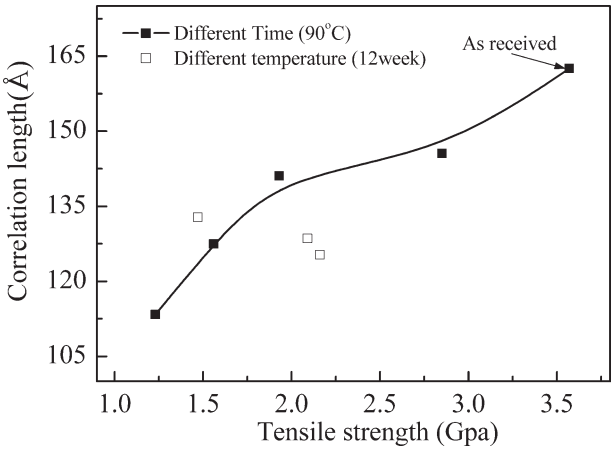

Figure 8. Relationship between L_c ($\mathbf{q} = 0.1$–0.2) and tensile strength.

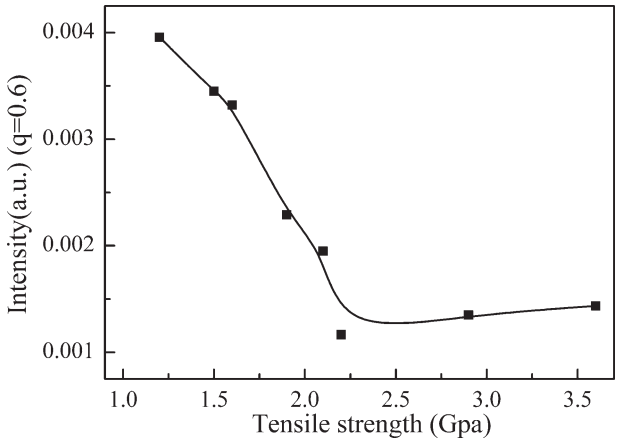

Figure 9. Relationship between the intensity of small nanovoids and tensile strength.

Potential Mechanisms of Hydrothermal Aging

The tensile strength and reduced viscosity values are presented in Table I. As previously mentioned, the presence of bonding ties and voids at different aging periods was confirmed via SAXS and DMTA. These results suggest that the hydrolysis involved two different phases. The relationship between the tensile strength and L_c is shown in Figure 8. The tensile strength increased with L_c at the same temperature. The chains easily slipped through the bonding ties between the fibrils under the tensile load. In addition, the tensile strength decreased after the hydrolysis of the bonding ties. However, no correlation was found between L_c and the tensile strength at the same aging time. The deterioration of the tensile strength may have been due to the presence of defects such as voids. The number of scatters was directly proportional to the intensity.[21] The relationship between the tensile strength and the intensity of void scattering ($\mathbf{q} = 0.6$) is shown in Figure 9. Few voids were detected in the initial stages, whereas the tensile strength decreased around 30%. This suggested that bonding tie collapse was the main hydrolysis mechanism in the initial stages. A linear relationship between the tensile strength and number of voids was observed; this indicated that the tensile strength was strongly affected by the number of defects.

A model based on fibrillar structures[4] is proposed to illustrate the potential mechanism of hydrothermal aging. The bonding ties were degraded at the initial stage of aging. Water diffusion into the crystal structure was slower than in the amorphous region because diffusion into the crystal interface took a longer time and required a higher temperature. Consequently, voids formed in the amorphous region rather than in the crystal regions.

CONCLUSIONS

Kevlar 129 was aged in deionized water at a moderate temperature. AFM analysis results reveal that the surface morphology changed slightly when the tensile strength was decreased by 70%. The potential mechanisms were investigated via SAXS and DMTA. The changes in L_c implied the occurrence of hydrolysis in the bonding ties. The bonding ties reformed when the fiber was heated to 250°C. The number and size of scatters in the fiber direction were independent of the aging temperature and time. Small voids (10 Å) formed after 12 weeks of aging at a high temperature; this indicated that the hydrolysis of the chain may have originated in the amorphous region rather than in the crystals. The proposed model suggests that the tensile strength was affected by the size of the bonding ties and the number of voids. Therefore, Ruland's streak method was useful in analyzing the voids of aramid fibers after aging. The method could be used to investigate the aging behavior of other fibers.

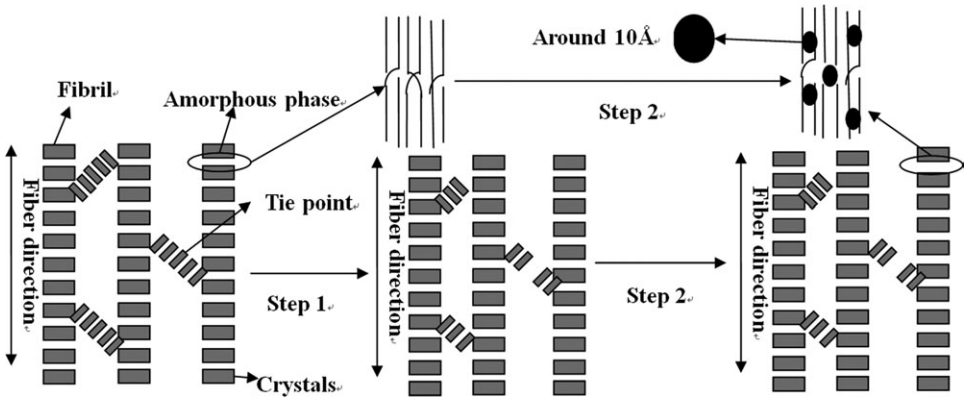

Figure 10. Possible mechanisms of hydrothermal aging.

ACKNOWLEDGMENTS

This work was supported by the Institute of High Energy Physics of the Chinese Academy of Sciences. We would also like to thank Dr. Guang Mo, Dr. Yu Gong, Dr. Hong-Zhi Li, and Dr. Zhong-Hua Wu for their assistance in the SAXS analysis and data collection. This work was supported by 863(2012AA03A209).

REFERENCES

1. Rao, Y.; Waddon, A.-J.; Farris, R.-J. *Polymer* **2001**, *42*, 5925.
2. Rao, Y.; Waddon, A.-J.; Farris, R.-J. *Polymer* **2001**, *42*, 5937.
3. Anjana, J.; Abhishek, S.; Sangappa, M. S.-S.; Somashekar, R. *J. Appl. Polym. Sci.* **2006**, *100*, 4910.
4. Panar, M.; Avakian, P.; Blume, R. C.; Gardner, K. H.; Gierke, T. D.; Yang, H. H. *J. Polym. Sci. Polym. Phys. Ed.* **1983**, *21*, 1955.
5. Dobb, M.-G.; Park, C.-R.; Robson, R.-M. *J. Mater. Sci.* **1992**, *27*, 3876.
6. Davies, R. J.; Koenig, C.; Burghammer, M.; Rieke, C. *Appl. Phys. Lett.* **2008**, *92*, 1.
7. Derombise, G.; van Schoors, L.; Vouyovitch, B. A.; Davies, P. *J. Appl. Polym. Sci.* **2012**, *123*, 3098.
8. Arrieta, C.; David, É.; Dolez, P.; Vu-Khanh, T. *Polym. Degrad. Stab.* **2011**, *96*, 1411.
9. Derombise, G.; Chailleux, E.; Forest, B.; Riou, L.; Lacotte, N.; Vouyovitch Van Schoors, L.; Davies, P. *Polym. Eng. Sci.* **2011**, *51*, 1366.
10. Forster, A. L.; Pintus, P.; Messin, G. H. R.; Riley, M. A.; Petit, S.; Rossiter, W.; Chin, J.; Rice, K. D. *Polym. Degrad. Stab.* **2011**, *96*, 247.
11. Derombise, G.; Van Schoors, L. V.; Davies, P. *J. Appl. Polym. Sci.* **2010**, *116*, 2504.
12. Derombise, B.; Van Schoors, L. V.; Messou, M. F.; Davies, P. *J. Appl. Polym. Sci.* **2010**, *117*, 888.
13. Derombise, G.; Van Schoors, L. V.; Davies, P. *Polym. Degrad. Stab.* **2009**, *94*, 1615.
14. Holmes, G. A.; Park, E. S. J. Presented at The 19th International Conference on Composites (ICCM-17), Edinburgh, Scotland, **2009**, July.
15. Arrieta, C.; David, E.; Dolez, P.; Vu-Khanh, T. *Polym. Compos.* **2011**, *32*, 362.
16. Zhang, P. H.; Zhang, J. C.; Chen, J. Y.; Hao, X. m.; Wang, S. Y.; Feng, X. X; Guo, Y. H.. *Polym. Degrad. Stab.* **2006**, *91*, 2761.
17. Arrieta, C.; David, E.; Dolez, P.; Vu-Khanh, T. *J. Appl. Polym. Sci.* **2010**, *115*, 3031.
18. Litvinov, V. M.; Xu, J.; Melian, C.; Demco, D. E.; Moller, M.; Simmelink, J. *Macromolecules* **2011**, *44*, 9254.
19. Londono, J. D.; Annadurai, V.; Gopalkrishne Urs, R.; Somashekar, R. *J. Appl. Polym. Sci.* **2002**, *85*, 2382.
20. Jiang, Z.; Tang, Y.; Rieger, J.; Enderle, H.; Lilge, D.; Roth, S. V.; Gehrke, R.; Wu, Z.; Li, Z.; Li, X.; Men, Y. *Eur. Polym. J.* **2010**, *46*, 1866.
21. Zhu, C.; Liu, X.; Yu, X.; Zhao, N.; Liu, J.; Xu, J. *Carbon* **2012**, *50*, 235.
22. Pauw, B. R.; Vigild, M. E.; Mortensen, K.; Andreasen, J. W.; Klop, E. A. *J. Appl. Crystallogr.* **2010**, *43*, 837.
23. Katsuya, F.; Yoshikiyo, H.; Tatsuro, H.; Asao, O.; Keiko, N. *Carbon* **2008**, *46*, 722.
24. Lozano-Castelló, D.; Raymundo-Piñero, E.; Cazorla-Amorós, D.; Linares-Solano, A.; Müller, M.; Riekel, C. *Carbon* **2002**, *40*, 2727.
25. Vickers, M.-E.; Briggs, N.-P.; Ibbett, R.-N.; Payne, J.-J.; Smith, S.-B. *Polymer* **2001**, *42*, 8241.
26. Crawshaw, J.; Cameron, R.-E. *Polymer* **2000**, *41*, 4691.
27. Wang, W.; Ruland, W.; Cohen, Y. *Acta Polym.* **1993**, *44*, 273.
28. Ruland, W. *J. Appl. Crystallogr.* **1971**, *4*, 70.
29. Li, C.-S.; Zhan, M.-S.; Huang, X. C.; Zhou, H. *J. Appl. Polym. Sci.* **2012**, *126*, 552.
30. Springer, H.; Obaid, A.-A.; Prabawa, A.-B.; Hinrichsen, G. *Text. Res. J.* **1998**, *68*, 588.
31. Grubb, D. T.; Prasad, K.; Adams, W. *Polymer* **1991**, *32*, 1167.
32. Rana, S.; Fanga, D.; Zonga, X. *Polymer* **2001**, *42*, 1601.